Feasibility of nanofluid-based optical filters

Robert A. Taylor,[1,*] Todd P. Otanicar,[2] Yasitha Herukerrupu,[1] Fabienne Bremond,[1] Gary Rosengarten,[3] Evatt R. Hawkes,[1] Xuchuan Jiang,[1] and Sylvain Coulombe[4]

[1]University of New South Wales, Sydney, New South Wales 2052, Australia

[2]The University of Tulsa, Tulsa, Oklahoma 74104, USA

[3]RMIT University, Melbourne, Victoria 3053, Australia

[4]McGill University, Montréal, Quebec H3A 0C5, Canada

*Corresponding author: Robert.Taylor@UNSW.edu.au

Received 17 December 2012; revised 20 January 2013; accepted 21 January 2013; posted 23 January 2013 (Doc. ID 181102); published 25 February 2013

In this article we report recent modeling and design work indicating that mixtures of nanoparticles in liquids can be used as an alternative to conventional optical filters. The major motivation for creating *liquid* optical filters is that they can be pumped in and out of a system to meet transient needs in an application. To demonstrate the versatility of this new class of filters, we present the design of nanofluids for use as long-pass, short-pass, and bandpass optical filters using a simple Monte Carlo optimization procedure. With relatively simple mixtures, we achieve filters with <15% mean-squared deviation in transmittance from conventional filters. We also discuss the current commercial feasibility of nanofluid-based optical filters by including an estimation of today's off-the-shelf cost of the materials. While the limited availability of quality commercial nanoparticles makes it hard to compete with conventional filters, new synthesis methods and economies of scale could enable nanofluid-based optical filters in the near future. As such, this study lays the groundwork for creating a new class of selective optical filters for a wide range of applications, namely communications, electronics, optical sensors, lighting, photography, medicine, and many more.

OCIS codes: 160.4236, 160.6840, 230.1360, 230.7408.

1. Introduction

Optical filters are used in a myriad of applications: communications, sensing, lighting, photography, and energy harvesting [1,2]. Today's optical filters are generally fabricated with some form of deposition onto *solid* substrates or by adding absorbing materials to transparent solids such as glasses and plastics [1,3]. This article introduces the idea of creating *liquid*-based optical filters using nanoparticles as the tuning vector. Such filters could potentially be pumped into and out of a system, enabling them to meet transient needs in an application. At the moment, however, liquid filters remain a relatively untapped area of research. To date, only a few "pure" fluid filters with tolerable optical properties have been studied [4,5].

The present work takes advantage of recent advances in nanofabrication techniques—including fabrication of nanosized particles—which have enabled a step change in the range of "nanoscale" products available [6,7]. We demonstrate herein that, by dispersing specifically engineered nanosized particles into liquids, it is possible to achieve the same level of control—in a liquid—as has been achieved for traditional solid filters. This article will describe the process for designing liquid filters that are appropriate for a wide variety of optical filtering applications. The motivation for the proposed particle suspension-based optical filters is that they can potentially provide more control than solid filters. Some advantages of the approach are that (a) particles can be mixed, matched, and changed to suit the

1559-128X/13/071413-10$15.00/0

application, (b) particle suspensions can easily and quickly be pumped out and replaced in a system, and (c) it is possible to dynamically control particle distributions and/or switch optical properties using magnetic/electric fields and/or by altering particle size.

Previous work has indicated that tunable optical properties can be obtained with properly designed dispersions of nanoparticles in conventional base fluids [8–17]. This study will expand on [9–17] to intentionally design nanofluid mixtures that can be used as *selective* absorbing fluids that match well with the conventional filters shown in Fig. 1. Thus, this study will present modeling work that indicates that short-pass, long-pass, and bandpass nanofluid-based filters are all possible. It is noteworthy that this variety is attainable using just one- and two-particle component mixtures, which we believe demonstrates the versatility of nanofluid filters.

Achieving highly selective filters requires careful design of the following parameters: materials (nanoparticles and fluids), the number of nanoparticle materials to combine in the filter, nanoparticle size, nanoparticle volume fraction, and the geometry of the filter. In this study, the "selectivity" or "success" of the resulting nanofluid filters is determined by calculating the mean-squared deviation from the conventional filters shown in Fig. 1.

2. Approach and Assumptions

In order to design these filters, the most important consideration is the choice of materials. To make this choice, we first reviewed the bulk optical properties of many different materials. Optical properties (such as the complex refractive indices) for most pure materials can be found in standard texts—e.g., the handbook edited by Palik [19]. Most materials are not suitable for optical filters as they are characterized by either broad absorption or absorption far away from optical wavelengths. Another requirement for an optical filter is that it must be stable over time. This further limits candidate materials to those that do not react or oxidize. For this reason, most can be eliminated from the pool of candidate materials for optical filters. It should be noted that advances in surface passivation/functionalization can be expected to one day add many more feasible, stable materials [20–22]. Based on our analysis of all potential candidates, we narrowed down to a short list of potential nanoparticles: noble metals and dielectric-core/noble-metal-shell nanoparticles [23]. Noble metals work well because they show strong absorption over a relatively narrow range of wavelengths due to plasmon resonance. Noble metals are also, by definition, resistant to oxidation and corrosion. This is desirable because the optical properties must be compatible with other materials in the system. Core/shell nanoparticles, with dielectric cores and noble metal shells, are another good possibility because they have even more pronounced plasmon absorption peaks than pure noble metals. Also, by controlling the ratio of shell-to-core radius, the resonance peak can be shifted considerably (see [23–27]). Core/shell particles are also advantageous because they use considerably less metal material. While synthesis of particles is not easy, many researchers have successfully created them via a variety of methods as is shown (below) in Table 1. A few core/shell particle formulations are even available off-the-shelf (OTS), but because of limited production volumes the cost is high (note that cost and reliability of these filters will be discussed in Section 5).

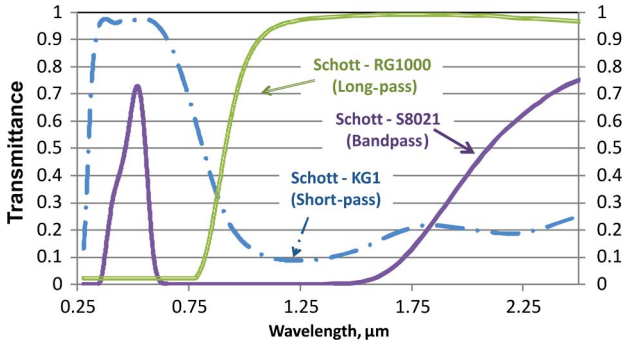

Fig. 1. (Color online) Selection of conventional filters to be matched in this study; data from Schott [18].

For optical filtration, we would ideally have our choice of a wide variety of "line" absorbers that achieve highly selective light extinction. Metallic shell/silica core particles were chosen because they approach this ideal with very pronounced plasmon resonance. That is, for certain optical wavelengths, the free electron gas (or plasma) at the surface of the nanoshell strongly absorbs incident photons. Therefore, a narrow band of wavelengths is converted into plasmon waves that spread across the surface. These "surface plasmons" are collective charge oscillations that occur at the interface between the shell (a conductor) and the core (a dielectric). The wavelength—or natural resonant frequency—at which this occurs is determined by parameters such as the particle's size, shape, shell thickness, and bulk optical properties of the materials involved [37]. Core/shell nanoparticles can then be tuned to achieve the desired optical properties by changing the above-mentioned parameters.

Depending on the application, any number of particles can theoretically be selected and combined into a filter. A key point that must be considered is that, when particles are mixed with a liquid, the liquid will also absorb light. Water and various organic liquids are effectively transparent at wavelengths longer than 0.3 μm and shorter than 1.5 μm but can be highly absorbing outside that range.

Nanoparticles with outer diameters in the 20–50 nm range were chosen to ensure the particles will follow the flow and not cause damage to pumps or plumbing. For reasonably thin nanofluid-based filters (i.e., 0.1 mm), the particle volume fraction required for effective absorption is in the range of 0%–0.01% [14]. For a relatively thick volumetric

Table 1. Selected Core/Shell Nanoparticle Fabrication Approaches

Article Title	Authors (Year)	Synthesis Method	Approximate Size (nm)[a]
Preparation and characterization of gold nanoshells coated with self-assembled monolayers	Pham *et al.* (2002) [28]	Multistep wet chemistry[b]	S, 30 nm AuC, 100 nm SiO_2
Synthesis of contiguous silica-gold core-shell structures: critical parameters and processes	Phonthammachai *et al.* (2007) [29]	Multistep wet chemistry[b]	S, 12–15 nm AuC, 100 nm SiO_2
Nanoshells made easy: improving Au layer growth on nanoparticle surfaces	Brinson *et al.* (2008) [30]	Multistep wet chemistry[b]	S, 10–50 nm AuC, 70–380 nm SiO_2(includes nanorice)
Scalable routes to gold nanoshells with tunable sizes and response to near-infrared pulsed-laser irradiation	Prevo *et al.* (2008) [31]	Multistep chemistry, galvanic replacement of Ag	S, 7 nm AuC, 20–70 nm hollow (base fluid)
Microwave absorption properties of the core/shell-type iron and nickel nanoparticles	Lu *et al.* (2008) [32]	DC arc discharge+ passivation in O_2	S, 5 nm Fe Oxide/Ni OxideC, 100 nm Fe/Ni
In situ catalytic encapsulation of core-shell nanoparticles having variable shell thickness: dielectric and energy storage properties of high-permittivity metal oxide nanocomposites	Li *et al.* (2010) [33]	Layer by layer coating, chemisorptive activation	S, variable thickness Al_2O_3C, 70, 140 nm ZrO_2, $BaTiO_3$
Synthesis and plasmonic properties of silver and gold nanoshells on polystyrene cores of different size and of gold-silver core-shell nanostructures	Yong *et al.* (2006) [34]	Multistep wet chemistry[b] (polystyrene beads purchased)	S, 30–50 nm Au/AgC, 188, 296, 543 nm polystyrene
Silver nanoshells: variations in morphologies and optical properties	Jackson and Halas (2001) [35]	Wet chemistry, silver particles grown directly or intermediary gold	S, 15–25 AgC, 120 nm SiO_2

[a]C, core diameter; S, shell thickness.

[b]Silica core (using the Stöber method) and small, 1–3 nm metal particles are fabricated separately (see [36]). These small particles are attached to the core via linkers. Uniform shells are grown using these as nucleation sites.

absorber (i.e., 100 mm), only low-volume fractions of particles ($<1\times10^{-7}\%$) are needed for sufficient absorption.

A. Absorption and Scattering Calculations

After the materials are selected, the next step is to modify the bulk properties based on particle and/or shell size. The Drude–Lorentz model is used to make these modifications, which has been demonstrated numerically [38] and confirmed experimentally for metallic nanoparticles [39]. This classical model assumes that electrons are harmonically bound to the nucleus and the following expression can be used [40–42]:

$$\varepsilon(\omega)=\varepsilon(\omega)_{\text{exp}}+\omega_p^2\frac{1}{\omega^2+i\omega\gamma_{\text{bulk}}}-\omega_p^2\frac{1}{\omega^2+i\omega\gamma(l_{\text{eff}})}, \tag{1}$$

where $\varepsilon(\omega)_{\text{exp}}$ is the bulk complex dielectric constant (from handbook data), ω_p is the bulk plasmon frequency, ω is the variable electromagnetic wave frequency, and γ_{bulk} is the relaxation frequency of the bulk metal. The small particle modification term, $\gamma(l_{\text{eff}})$, is defined as [43,44]

$$\gamma(l_{\text{eff}})=\frac{1}{\tau_o}+\frac{AV_f}{D}. \tag{2}$$

In this equation, τ_o is the bulk metal free electron scattering time, A is geometric parameter we assume to be 1 [38], V_f is the Fermi velocity (where an experimental value of the order of $V_f\sim10^6$ m/s is used [45]), and D is the particle diameter that (when appropriate) is used as the effective mean free path. The reason for taking this extra step is that room temperature metals can have electron mean free paths (the average distance an electron goes between two scattering events) of the order of the diameter of the nanoparticles. For example, copper and silver have electron mean free paths around 50 nm [46]. Thus, Eqs. (1) and (2) were used to modify the bulk properties to account for small sized particles.

To model core/shell nanoparticles, we used the quasi-static approach given in [42]. This assumption is valid if particles are much smaller than the wavelength of light *and* if the incident light flux does not vary over the particle diameter. Both of these conditions are easily satisfied with nanoparticles. Once the dielectric constants and refractive indices are known, we can calculate optical coefficients. As long as the particles are small and far apart, we can assume that the particles are independent of each other. This assumption is valid for the low-volume fractions used herein and allows for the Rayleigh approximation to be made (see [10]). In this regime it is relatively straightforward to use the approach of [42,47] to calculate the scattering, $Q_{\text{scat\_}i}$, absorption, $Q_{\text{abs\_}i}$, and extinction, $Q_{\text{ext\_}i}$, efficiencies of individual particles. The challenging step in this approach is to select potential nanoparticle options based on optical properties from the library of candidate materials. Figure 2 shows a small subset (which spans the optical spectrum), demonstrating the variety of

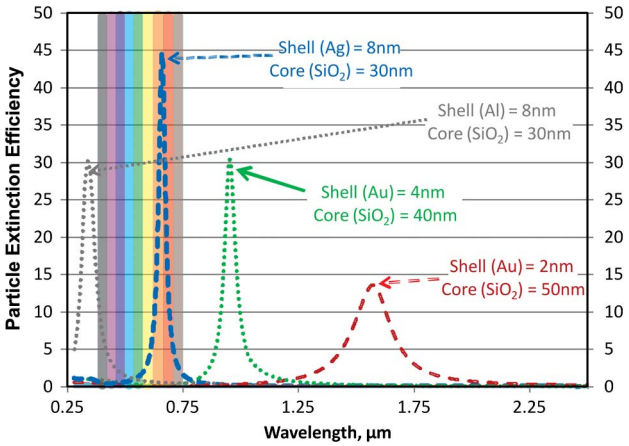

Fig. 2. (Color online) Small selection of the library of nanoparticle options available. Extinction efficiency (which includes both absorption and scattering) is plotted as a function of wavelength.

nanoparticle options that were found using this theoretical approach.

B. Optimization

Above, we identified the absorption and scattering of individual particles. To achieve the desired filters, we need to determine the correct nanoparticles recipe to be used—i.e., *how much* of each nanoparticle material to add to the liquid filter. Using the Rayleigh approximation, it is possible to simply add up the extinction coefficient of all nanoparticles. Thus, we can calculate the extinction coefficient of each component particle based on the volume fraction, f_v, of the particle by the following equation [47]:

$$\sigma_{\text{particle\_}i} = \frac{3}{2}\frac{f_v Q_{\text{ext\_}i}}{D}. \tag{3}$$

By the same logic, we propose that the contributions of all particles in the system can be summed to get a total extinction coefficient from N particles:

$$\sigma_{\text{particles}} = \sum_{1}^{N} \sigma_{\text{particle\_}i}. \tag{4}$$

It should be noted that the base fluid can contribute to the extinction of light as it passes through a nanofluid. As a first-order approximation, we assume the total nanofluid extinction coefficient is a simple addition of the base fluid extinction coefficient and that of the particles:

$$\sigma_{\text{total}} = \sigma_{\text{particles}} + \sigma_{\text{fluid}}. \tag{5}$$

This assumption has been validated experimentally for low-volume fractions in water (see [14]). Although other approaches to calculate how much light is transmitted through the filter are possible (e.g., [48]), assuming a nonscattering liquid base fluid, we use Beer's law [47],

$$T = \frac{I}{I_o} = e^{-L\sigma_{\text{total}}}, \tag{6}$$

where T is the transmittance, I is the transmitted irradiation, I_o is the incident irradiation, and L is the length of the light path in the filter. It should be stated that the transmittance calculated includes scattering. These are not differentiated, but the extinction is mostly due to absorption ($Q_{\text{abs\_}i}$:$Q_{\text{scat\_}i}$ ~ 10:1) in the modeling in this study. However, if desirable, it is possible to create a nanofluid filter that is highly scattering. That is, selected wavelengths of the incident light can, theoretically, be scattering away from the propagation direction, but this is outside the scope of this work. To determine the effectiveness of these filters, where $\zeta|0 \le \zeta \le 1$, the following simple integral for mean-squared deviation is used:

$$\zeta_{\text{nano-conv}} = 1 - \frac{\int_{\lambda_{\text{short}}}^{\lambda_{\text{long}}} (T_{\text{nano}} - T_{\text{conv}})^2 \mathrm{d}\lambda}{\lambda_{\text{long}} - \lambda_{\text{short}}}, \tag{7}$$

where T is the transmittance and λ is the wavelength. Equation (7) is simply the mean-squared deviation from the conventional filter (normalized over the wavelength range). Thus, this becomes our objective function for filter optimization. A simple Monte Carlo approach is used to randomly generate volume fraction combinations (over a range of assumed values). For each filter design, these random results are then sorted by applying Eq. (7) to find the maximum filter effectiveness.

3. Results

By optimizing mixtures of the nanoparticles via the effectiveness given in Eq. (7), it is possible to obtain nanofluid filters that approach conventional filters. Figures 3–5 show our results for optimum nanofluid filters as compared to their baseline conventional filters. Results are plotted across wavelengths from the near UV to the near IR, 0.25–2.5 μm. The transmittance (between 0 and 1) of the filter is compared to the ideal filter on the left y axis, while the extinction efficiency of the nanoparticles used in the filter

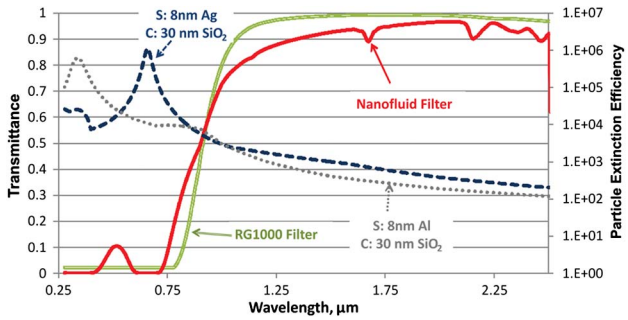

Fig. 3. (Color online) Comparison of a conventional thin film long-pass filter (Schott's RG1000 [18]) to a nanofluid long-pass filter (Therminol VP-1 as the base fluid). Solid curves represent filter transmittance and correspond to the left axis, while dashed and dotted curves correspond to the right axis.

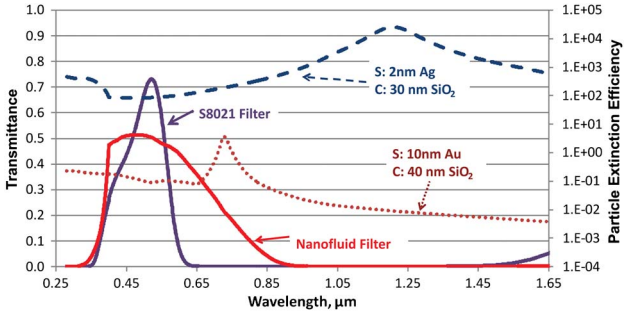

Fig. 4. (Color online) Comparison of a conventional thin film bandpass filter (Schott's S8021 [18]) to a nanofluid bandpass filter (Therminol VP-1 as the base fluid). Solid curves represent filter transmittance and correspond to the left axis, while dashed and dotted curves correspond to the right axis.

is shown on the right y axis. In Figs. 3–5, the solid curves represent filters (corresponding to the left y axis) and dotted curves represent particles (corresponding to the right y axis). It can be seen in Fig. 3 that it is possible to achieve roughly the same transmission as the commercial long-pass filter with a two-nanoparticle nanofluid. It is expected that, with more complicated nanoparticle combinations (<2 nanoparticle types), sharper filtration bands would be possible. Figures 4 and 5 show that effective bandpass and short-pass filter designs are also possible through the use of engineered nanofluids. As might be anticipated, the bandpass filter was hardest to match, achieving an effectiveness of only 85%. Overall, a reasonably good match with conventional filters can be achieved.

Table 2 summarizes the nanoparticle volume fractions and effectiveness of the filters achieved in this study. It can be seen in Table 2 that, in these designs, the highest nanoparticle volume fraction is actually quite low; f_v is 5.1×10^{-4} or 0.05% volume of particles per volume of liquid. This means very few nanoparticles are needed to create these filters.

4. Discussion

While the theoretical model predicts relatively good results, novel nanofluid filters are far from being commercially viable. In practice, the filters shown in Table 2 are difficult to obtain. The following fabrication challenges must be overcome (or in some way bypassed) in order to fabricate nanofluid optical filters:

i. Tight size distribution tolerances (in shell thickness and polydispersity).
ii. Small nanoshells (<50 nm, dielectric core, metal shell).
iii. Thin, uniform shell coatings.
iv. Long lifetime/stability/noncoagulating.
v. Low U.S. dollars/m^2 nanoparticle synthesis methods.

Significant research work has already gone into addressing each of these challenges [50–62] for nanoparticles in general. Only a brief discussion of these limitations is presented here, but the interested reader can refer to the works cited in the proceeding discussion and tables.

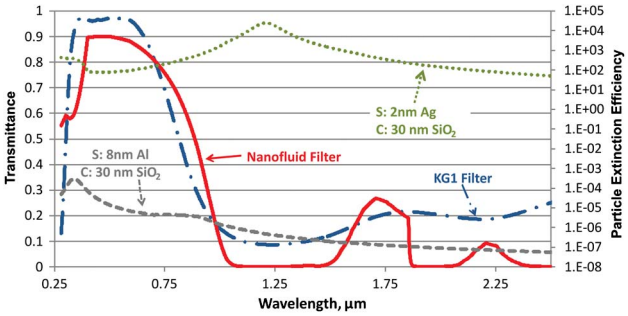

Fig. 5. (Color online) Comparison of a conventional thin film short-pass filter (Schott's KG1 [18]) to a nanofluid short-pass filter (water as the base fluid). Solid and long dashed–dotted curves represent filter transmittance and correspond to the left axis, while dashed and dotted curves correspond to the right axis.

A. Tight Size Distribution Tolerances

This article highlights the fact that small deviations in the ratio of the outer diameter to the inner diameter give rise to tunable optical filtration. This same phenomenon, unfortunately, also presents a huge challenge. In the model above, the particles were assumed to be uniform in terms of both outer diameter and shell thickness. For effective filtration there is little tolerance for distributions in either of these dimensions. Figure 2 shows that changing a gold nanoshell from having dimensions of 40 nm core/4 nm shell to 50 nm core/2 nm shell will shift the peak absorption by approximately 600 nm, all other parameters being equal. Thus, a tolerance of $<\pm 1$ nm in shell thickness and $<\pm 1\%$ in the core/shell radius ratio may be required in some cases to achieve the filters presented in Table 2. In reality, there will be some distribution of particle sizes, even in a stable suspension since the nanoparticles cannot be made to be entirely monodisperse. Size distributions can be accounted for by adding a probability density function into the extinction coefficient calculated in Eq. (3), see Averitt *et al.* who assume an 18%–20% deviation from the mean size [63]. This serves to broaden the peaks shown in Fig. 2.

B. Small Nanoshells

A literature review of gold nanoshells revealed that, to date, the smallest achievable particles are of the order of 60 nm. Comparing Table 1 with Table 2 reveals that very little of the literature reports small cores and/or thin shells (<10 nm), which are needed for the materials used in this study. The most common method for making silica cores utilizes the Stöber process [64] to obtain a monosized distribution of particles. This relatively simple chemical process is used to precipitate nanoparticles from a mixture of reactants and is generally limited to particle sizes >50 nm, which are larger than the particles needed. Since the goal of this study is to create an absorbing filter, smaller particles are desired.

Table 2. Summary of This Study's Designed Liquid Nanofluid Optical Filters as Compared to Conventional Solid Filters[a]

Solid Filters	Approximate Solid Filter Cost (U.S. Dollars/m^2)[b]	Particle 1 (f_{v1})[c]	Particle 2 (f_{v2})[c]	Base Fluid Thickness	Nanofluid Filter ζ(%)	Approximate Nanofilter Cost: Current OTS {10X Raw Material} (U.S. Dollars/m^2)
GC435 [41]	16,632	S, 8 nm AuC, 30 nm SiO_2(9.5×10^{-5})	None	Therminol VP-1 (0.04 mm)	94.0	1310 {11}
OG570 [41]	16,632	S, 8 nm AlC, 30 nm SiO_2(9.5×10^{-5})	Pure 30 nm Au(9.6×10^{-5})	Therminol VP-1 (0.06 mm)	91.0	465 {34}
RG1000 [41]	18,480	S, 8 nm AgC, 30 nm SiO_2(6.0×10^{-4})	8 nm Al 30 nm SiO_2(5.1×10^{-4})	Therminol VP-1 (0.05 mm)	91.8	7530 {1.00}
S8021 [41]	16,632	S, 10 nm AuC, 40 nm SiO_2(2.2×10^{-9})	2 nm Ag 30 nm SiO_2(4.6×10^{-5})	Therminol VP-1 (8.1 mm)	85.0	94,150 {14.40}
KG1 [41]	14,784	S, 2 nm AgC, 30 nm SiO_2(3.15×10^{-5})	S, 8 nm AgC, 40 nm SiO_2(2×10^{-13})	H_2O(1.4 mm)	97.8	2560 {0.31}

[a]Some filters do not appear in the figures.
[b]Conventional filter cost from [49].
[c]C, core diameter; S, shell thickness.

This is needed since scattering is proportional to diameter to the fourth power, while absorption is linearly related to diameter (in the Rayleigh limit).

Small particles of a single material (i.e., pure Au), on the other hand, can easily be obtained and match well with theory. There are a number of suppliers for OTS nanoparticles, such as those used in Figs. 6A and 6C. On the other hand, the small core/shell particles needed in Table 2 are not yet widely reported in research or available OTS. To test optical properties of state-of-the-art commercially available nanoparticles, some custom gold nanoshells (~120 nm outside diameter) were purchased from NanoComposix (USA) [65]. The shell thickness

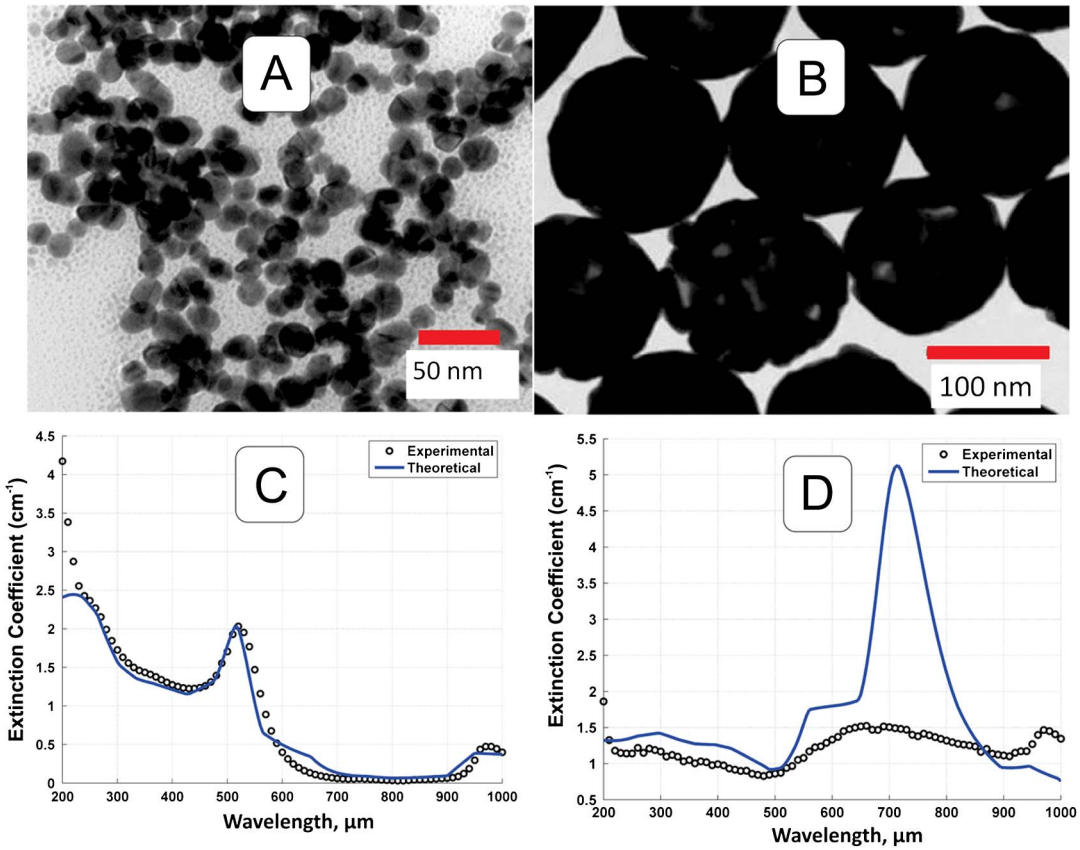

Fig. 6. (Color online) TEM of (A) 10 nm (mean diameter) gold nanoparticles and (B) 120 nm (mean outer diameter) gold/silica nanoparticles. Experiments (circles) versus modeling (solid lines) results of extinction coefficients, σ_{total} from Eq. (5), for (C) a PVP stabilized aqueous suspension of gold nanoparticles of image (A) at 2.7×10^{12} particles/mL and (D) a PVP stabilized aqueous suspension of gold/silica nanoparticles of image (B) at 5.9×10^{9} particles/mL. Note that particles were purchased from NanoComposix [68].

was quoted from the manufacturer to be ~25 nm, which is in line with many of the results reported in the literature. The results for these particles, however, were not acceptable for the filters shown in Table 2. While the transmission electron microscopy (TEM) images of Fig. 6D show the particle size as being relatively uniform, this changes when the particles are dispersed in water. When aqueous samples are tested with a NanoSight LM10 HS [66], we observed larger particles than the manufactured stated mean value with standard deviation nearing the mean diameter. These changes broaden the absorption peak and ultimately do not provide the line absorbers shown in Fig. 2. The results for these particles, therefore, were not deemed acceptable for the filters shown in Table 2.

C. Thin, Uniform Shells

The most commonly reported synthesis process for gold nanoshells requires small, 1–3 nm, gold "seed" particles to be attached to the core. These then serve as nucleation sites for shell growth. In this fabrication method it is important to grow the nucleation sites until the shell coats the entire core, which leads to larger thicknesses than the seed particles. Obtaining very thin shells is possible with this approach (see [67]), but an additional controlled subtractive step might be needed to obtain the thin shells used in Table 2.

Figures 6A and 6B show some characteristic TEM images of OTS nanoparticles from NanoComposix [68], while Figs. 6C and 6D show modeled and experimental results that we obtained in this research. (Note that the image shows nanoparticles at a considerably higher density than that at which they were tested once in fluid suspension.) While the TEM images of Fig. 6 show the particle size as being relatively uniform, the thin shells are generally very rough as is shown in the TEM of Fig. 6B. In addition, the core/shell nanoparticles tested in Fig. 6D did not match with models. The results for these particles, again, were not deemed acceptable for the filters shown in Table 2.

D. Long Lifetime/Stability

For reliable operation, nanoparticles must maintain their size for time scales of the order of years. Many approaches have been used to obtain stable colloidal suspensions [69–71]. Surfactants are probably the most commonly used method in the literature, and some of them have been shown to have little effect on nanofluid optical properties [14]. However, minor changes in surface chemistry, or size through particle agglomeration, could significantly change the optical properties. For example, particles functionalized with polyvinylpyridine (PVP) have been found to significantly suppress (and redshift) plasmon resonance in core/shell particles with thin shells due to dielectric screening [67].

While colloidal stability over time is a well-studied phenomenon, the optical filters proposed herein require some unique considerations. The selected core/shell nanoparticle fabrication techniques of Table 1 reported stable suspensions, but little information is given as to how stable these may be in an application. Thermal cycling (via absorption of light), exposure to intense light, compatibility of different nanoparticles types, and other factors can potentially destroy what was otherwise a stable nanofluid.

Since these filters absorb a significant portion of the light, we presume that the nanofluid filters (depending on the light's intensity) will undergo some amount of thermal cycling during usage. Thus, to investigate thermal stability, accelerated conditions in an experiment where the samples were repeatedly heated to 85°C was used to investigate this effect. Figure 7 shows the results of this test for up to 200 cycles for aqueous gold nanoparticle samples stabilized with PVP. It was found that, on average, the samples used in this study provided good stability during these thermal cycling tests. Note here that the effect of thermal cycling on the nanofluid stability is not frequently reported in the literature.

E. Cost Competitive

Currently, the types of nanoparticles which could potentially be used for these filters widely vary—costing between 288/g (gold nanopowder from Sigma Aldrich) and 32,000/g (custom made NanoXact silica/gold nanoshells from [65]) for OTS products. (Note that all dollar amounts are given in U.S. dollars.) Since the average price for gold bullion in 2013 was ~55/g, the majority of the cost is associated with producing nanoscale material. To estimate today's cost, we assume that these two prices apply for pure nanoparticles (288/g) and nanoshells (32,000/g), respectively. Since some of the particles needed for this filter are not currently available, these are merely rough estimates. To conservatively estimate the lowest potential future cost for these filters, a second (bracketed) cost is given in Table 2. For this case, we assume that total filter cost will be 10 times the cost of the raw materials needed to produce them; e.g., if 1 g of gold is needed, it would cost 550. Either way, the nanofluid filters usually provide a lower-cost option than conventional solid filters.

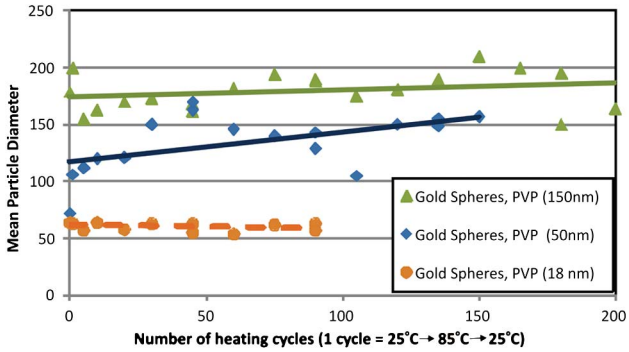

Fig. 7. (Color online) Thermal cycling experimental study of gold nanofluids.

5. Conclusions and Future Work

In this study we presented a first look at nanofluid-based filters that perform in optical wavelengths. As a case study, this research demonstrates that these filters provide an excellent platform to be employed in many applications. A big advantage of liquid filters is that they can potentially be controlled dynamically with pumps, magnetic/electric fields, or temperature. Based on the optimization results of this study, we can conclude that nanofluid optical filters can potentially be produced at relatively low cost. This is because, at most, only 0.001% particle volume fraction is required to achieve the designs presented herein. Also, for the core/shell nanoparticles used in this study, only a small fraction of each particle is a metal, while the majority is made of low-cost silica. Thus, the nanoparticles themselves can theoretically be fabricated at relatively low cost with less expensive synthesis methods. Since the average 2013 price for gold bullion is ~55/g, the prices charged by commercial nanoparticle suppliers are mainly due to nanoscale fabrication cost. However, researchers around the world are improving and developing many new nanofabrication techniques each year. Thus, while the tight control of particle size and shell thickness needed for our designs are not currently commercially available, this might be expected in the near future. Overall, this study shows that, with further optimization, nanofluid-based filters can provide a viable alternative to conventional optical filters. The goal of this study was to demonstrate the versatility and explore the feasibility of these filters, but through this, several other potential avenues for future work have been identified: (i) addition of more nanoparticle types to improve the effectiveness of the filters, (ii) experimental studies to validate the modeled optical properties, (iii) fine tuning for other optical applications such as lasing [72], photoacoustic imaging [73], and cancer treatments [74], and (iv) economic optimization to determine the real price of fabrication of the nanofluid-based filters and the relative value versus conventional filters in application.

R. A. T., E. R. H., and G. R. gratefully acknowledge the support of the ASI 2-A017 and the UNSW ECR program. T. P. O. gratefully acknowledges support from NSF grant CBET-1262201.

References

1. L. Martinu and D. Poitras, "Plasma deposition of optical films and coatings: a review," J. Vac. Sci. Technol. A **18**, 2619–2645 (2000).
2. A. G. Imenes and D. R. Mills, "Spectral beam splitting technology for increased conversion efficiency in solar concentrating systems: a review," Sol. Energy Mater. Sol. Cells **84**, 19–69 (2004).
3. S. Zaitsu, T. Jitsuno, M. Nakatsuka, T. Yamanaka, and S. Motokoshi, "Optical thin films consisting of nanoscale laminated layers," Appl. Phys. Lett. **80**, 2442–2444 (2002).
4. J. Kaluza, K.-H. Funken, U. Groer, A. Neumann, and K.-J. Riffelmann, "Properties of an optical fluid filter: theoretical evaluations and measurement results," J. Phys. IV **09**, Pr3-655–Pr3-660 (1999).
5. M. A. Chendo, M. R. Jacobson, and D. E. Osborn, "Liquid and thin-film filters for hybrid solar energy conversion systems," Solar Wind Technol. **4**, 131–138 1987).
6. J. Henzie, J. Lee, M. H. Lee, W. Hasan, and T. W. Odom, "Nanofabrication of plasmonic structures," Annu. Rev. Phys. Chem. **60**, 147–165 (2009).
7. R. Taylor, S. Coulombe, T. Otanicar, P. Phelan, A. Gunawan, W. Lv, G. Rosengarten, R. Prasher, and H. Tyagi, "Small particles, big impacts: a review of the diverse applications of nanofluids," J. Appl. Phys. **113**, 011301 (2013).
8. R. A. Taylor, T. P. Otanicar, and G. Rosengarten, "Nanofluid-based optical filter optimization for PV/T systems," Light Sci. Appl. **1**, 1–7 (2012).
9. T. P. Otanicar, P. E. Phelan, and J. S. Golden, "Optical properties of liquids for direct absorption solar thermal energy systems," Sol. Energy **83**, 969–977 (2009).
10. T. P. Otanicar, P. E. Phelan, R. S. Prasher, G. Rosengarten, and R. A. Taylor, "Nanofluid-based direct absorption solar collector," J. Renewable Sustainable Energy **2**, 033102 (2010).
11. T. P. Otanicar, I. Chowdhury, R. Prasher, and P. E. Phelan, "Band-gap tuned direct absorption for a hybrid concentrating solar photovoltaic/thermal system," J. Sol. Energy Eng. **133**, 041014 (2011).
12. T. P. Otanicar, P. E. Phelan, R. A. Taylor, and H. Tyagi, "Spatially varying extinction coefficient for direct absorption solar thermal collector optimization," J. Sol. Energy Eng. **133**, 024501 (2011).
13. T. P. Otanicar, R. A. Taylor, P. E. Phelan, and R. S. Prasher, "Impact of size and scattering mode on the optimal solar absorbing nanofluid," in *Proceedings of the ASME 2009 3rd International Conference of Energy Sustainability* (American Society of Mechanical Engineers (ASME), 2009), pp. 1–6.
14. R. A. Taylor, P. E. Phelan, T. P. Otanicar, R. Adrian, and R. Prasher, "Nanofluid optical property characterization: towards efficient direct absorption solar collectors," Nanoscale Res. Lett. **6**, 225 (2011).
15. R. A. Taylor, P. E. Phelan, T. P. Otanicar, C. A. Walker, M. Nguyen, S. Trimble, and R. Prasher, "Applicability of nanofluids in high flux solar collectors," J. Renewable Sustainable Energy **3**, 023104 (2011).
16. R. A. Taylor, P. E. Phelan, T. Otanicar, R. J. Adrian, and R. S. Prasher, "Vapor generation in a nanoparticle liquid suspension using a focused, continuous laser beam," Appl. Phys. Lett. **95**, 161907 (2009).
17. W. Lv, P. E. Phelan, R. Swaminathan, T. P. Otanicar, and R. A. Taylor, "Multifunctional core-shell nanoparticle suspensions for efficient absorption," J. Sol. Energy Eng. **135**, 021005 (2013).
18. Schott, "Optical filters" (2012), retrieved 10 March 2012, http://www.schott.com/advanced_optics/english/filter/index.html?PHPSESSID=ra0uavqiou413sfj003ublirj4.
19. E. D. Palik, *Handbook of Optical Constants of Solids* (Academic, 1997), Vol. **575**, p. 999.
20. M. A. G. Soler, S. W. da Silva, V. K. Garg, A. C. Oliveira, R. B. Azevedo, A. C. M. Pimenta, E. C. D. Lima, and P. C. Morais, "Surface passivation and characterization of cobalt-ferrite nanoparticles," Surf. Sci. **575**, 12–16 (2005).
21. K. K. Fung, B. Qin, and X. X. Zhang, "Passivation of a-Fe nanoparticle by epitaxial g-Fe_2O_3 shell," Mater. Sci. Eng. A **286**, 135–138 (2010).
22. J. Tavares, E. J. Swanson, and S. Coulombe, "Plasma synthesis of coated metal nanoparticles with surface properties tailored for dispersion," Plasma Processes Polym. **5**, 759–769 (2008).
23. N. J. Halas, S. Lal, W.-S. Chang, S. Link, and P. Nordlander, "Plasmons in strongly coupled metallic nanostructures," Chem. Rev. **111**, 3913–3961 (2011).
24. S. Zou, N. Janel, and G. C. Schatz, "Silver nanoparticle array structures that produce remarkably narrow plasmon lineshapes," J. Chem. Phys. **120**, 10871–10875 (2004).
25. G. Garcia, R. Buonsanti, E. L. Runnerstrom, R. J. Mendelsberg, A. Llordes, A. Anders, T. J. Richardson, and D. J. Milliron, "Dynamically modulating the surface plasmon resonance of doped semiconductor nanocrystals," Nano Lett. **11**, 4415–4420 (2011).

26. S. Zou and G. C. Schatz, "Narrow plasmonic/photonic extinction and scattering line shapes for one and two dimensional silver nanoparticle arrays," J. Chem. Phys. **121**, 12606–12612 (2004).
27. N. Palombo and K. Park, "Investigation of dynamic near-field radiation between quantum dots and plasmonic nanoparticles for effective tailoring of the solar spectrum," in *Proceedings of ASME 2011 International Mechanical Engineering Congress and Exposition* (American Society of Mechanical Engineers (ASME), 2011), pp. 1–5.
28. T. Pham, J. B. Jackson, N. J. Halas, and T. R. Lee, "Preparation and characterization of gold nanoshells coated with self-assembled monolayers," Langmuir **18**, 4915–4920 (2002).
29. N. Phonthammachai, J. C. Y. Kah, G. Jun, C. J. R. Sheppard, M. C. Olivo, S. G. Mhaisalkar, and T. J. White, "Synthesis of contiguous silica-gold core-shell structures: critical parameters and processes," Langmuir **24**, 5109–5112 (2008).
30. B. E. Brinson, J. B. Lassiter, C. S. Levin, R. Bardhan, N. Mirin, and N. J. Halas, "Nanoshells made easy: improving Au layer growth on nanoparticle surfaces," Langmuir **24**, 14166–14171 (2008).
31. B. G. Prevo, S. A. Esakoff, A. Mikhailovsky, and J. A. Zasadzinski, "Scalable routes to gold nanoshells with tunable sizes and response to near-infrared pulsed-laser irradiation," Small **4**, 1183–1195 (2008).
32. B. Lu, X. L. Dong, H. Huang, X. F. Zhang, X. G. Zhu, J. P. Lei, and J. P. Sun, "Microwave absorption properties of the core/shell-type iron and nickel nanoparticles," J. Magn. Magn. Mater. **320**, 1106–1111 (2008).
33. Z. Li, L. A. Fredin, P. Tewari, S. A. DiBenedetto, M. T. Lanagan, M. A. Ratner, and T. J. Marks, "In situ catalytic encapsulation of core-shell nanoparticles having variable shell thickness: dielectric and energy storage properties of high-permittivity metal oxide nanocomposites," Chem. Mater. **22**, 5154–5164 (2010).
34. K.-T. Yong, Y. Sahoo, M. T. Swihart, and P. N. Prasad, "Synthesis and plasmonic properties of silver and gold nanoshells on polystyrene cores of different size and of gold-silver core-shell nanostructures," Colloids Surf. A **290**, 89–105 (2006).
35. J. B. Jackson and N. J. Halas, "Silver nanoshells: variations in morphologies and optical properties," J. Phys. Chem. B **105**, 2743–2746 (2001).
36. D. G. Duff, A. Baiker, and P. P. Edwards, "A new hydrosol of gold clusters. 1. Formation and particle size variation," Langmuir **9**, 2301–2309 (1993).
37. L. K. Kelly, E. Coronado, L. L. Zhao, and G. C. Schatz, "The optical properties of metal nanoparticles: the influence of size, shape, and dielectric environment," J. Phys. Chem. B **107**, 668–677 (2003).
38. U. Kreibig and V. Vollmer, *Optical Properties of Metal Clusters*, 1st ed. (Springer, 2010).
39. R. Averitt, D. Sarkar, and N. Halas, "Plasmon resonance shifts of Au-coated Au_2S nanoshells: insight into multicomponent nanoparticle growth," Phys. Rev. Lett. **78**, 4217–4220 (1997).
40. A. E. Neeves and M. H. Birnboim, "Composite structures for the enhancement of nonlinear-optical susceptibility," J. Opt. Soc. Am. B **6**, 787–796 (1989).
41. M. Fox, *Optical Properties of Solids*, 2nd ed. (Oxford University, 2010), Chap. 7, pp. 180–210.
42. W. Lv, T. P. Otanicar, P. E. Phelan, L. Dai, R. A. Taylor, and R. Swaminathan, "Surface plasmon resonance shifts of a dispersion of core-shell nanoparticles for efficient solar absorption," in *Proceedings of Micro/Nanoscale Heat & Mass Transfer International Conference* (American Society of Mechanical Engineers (ASME), 2012), pp. 1–9.
43. P. B. Johnson and R. W. Christy, "Optical constants of the noble metals," Phys. Rev. B **6**, 4370–4379 (1972).
44. N. K. Grady, N. J. Halas, and P. Nordlander, "Influence of dielectric function properties on the optical response of plasmon resonant metallic nanoparticles," Chem. Phys. Lett. **399**, 167–171 (2004).
45. C. Kittel, *Introduction to Solid State Physics*, 8th ed. (Wiley, 2004), pp. 221–252.
46. C. N. Berglund and W. E. Spicer, "Photoemission studies of copper and silver: theory," Phys. Rev. **136**, A1030–A1044 (1964).
47. C. F. Bohren and D. R. Huffman, *Absorption and Scattering of Light by Small Particles* (Wiley-VCH, 1998), p. 544.
48. S. G. Moiseev, "Nanocomposite-based ultrathin polarization beamsplitter," Opt. Spectrosc. **111**, 233–240 (2011).
49. UQG, "Schott colour glass stock optical filters, order online" 2012, retrieved 17 December 2012, http://www.optical-filters.com/Schott_Filters.aspx.
50. Z. Liang, A. Susha, and F. Caruso, "Gold nanoparticle-based core—shell and hollow spheres and ordered assemblies thereof," Chem. Mater. **15**, 3176–3183 (2003).
51. M. Zhang, M. Drechsler, and A. H. E. Müller, "Template-controlled synthesis of wire-like cadmium sulfide nanoparticle assemblies within core–shell cylindrical polymer brushes," Chem. Mater. **16**, 537–543 (2004).
52. M. A. Nash, J. J. Lai, A. S. Hoffman, P. Yager, and P. S. Stayton, ""Smart" diblock copolymers as templates for magnetic-core gold-shell nanoparticle synthesis," Nano Lett. **10**, 85–91 (2010).
53. L. Lu, G. Sun, H. Zhang, H. Wang, S. Xi, J. Hu, Z. Tian, and R. Chen, "Fabrication of core-shell Au-Pt nanoparticle film and its potential application as catalysis and SERS substrate," J. Mater. Chem. **14**, 1005 (2004).
54. T. Roques-Carmes, F. Aldeek, L. Balan, S. Corbel, and R. Schneider, "Aqueous dispersions of core/shell CdSe/CdS quantum dots as nanofluids for electrowetting," Colloids Surf. A **377**, 269–277 (2011).
55. A. Abou-Hassan, R. Bazzi, and V. Cabuil, "Multistep continuous-flow microsynthesis of magnetic and fluorescent gamma-Fe_2O_3@SiO_2 core/shell nanoparticles," Angew. Chem. Int. Ed. Engl., Suppl. **48**, 7180–7183 (2009).
56. J. M. Pringle, O. Winther-Jensen, C. Lynam, G. G. Wallace, M. Forsyth, and D. R. MacFarlane, "One step synthesis of conducting polymer-noble metal nanoparticle composites using an ionic liquid," Adv. Funct. Mater. **18**, 2031–2040 (2008).
57. K. Kaneda, T. Mitsudome, T. Mizugaki, and K. Jitsukawa, "Development of heterogeneous olympic medal metal nanoparticle catalysts for environmentally benign molecular transformations based on the surface properties of hydrotalcite," Molecules **15**, 8988–9007 (2010).
58. N. Zheng and G. D. Stucky, "A general synthetic strategy for oxide-supported metal nanoparticle catalysts," J. Chem. Am. Soc. **128**, 14278–14280 (2006).
59. M. Grzelczak, J. Pérez-Juste, P. Mulvaney, and L. M. Liz-Marzán, "Shape control in gold nanoparticle synthesis," Chem. Soc. Rev. **37**, 1783–1791 (2008).
60. T. C. Wang, M. F. Rubner, and R. E. Cohen, "Polyelectrolyte multilayer nanoreactors for preparing silver nanoparticle composites: controlling metal concentration and nanoparticle size," Langmuir **18**, 3370–3375 (2002).
61. K.-S. Kim, D. Demberelnyamba, and H. Lee, "Size-selective synthesis of gold and platinum nanoparticles using novel thiol-functionalized ionic liquids," Langmuir **20**, 556–560 (2004).
62. K. R. Gopidas, J. K. Whitesell, M. A. Fox, and N. Carolina, "Catalytic applications of a palladium-nanoparticle-cored dendrimer," Nano Lett. **3**, 1–4 (2003).
63. R. D. Averitt, S. L. Westcott, and N. J. Halas, "Linear optical properties of gold nanoshells," J. Opt. Soc. Am. B **16**, 1824–1832 (1999).
64. W. Stöber, A. Fink, and E. Bohn, "Controlled growth of monodisperse silica spheres in the micron size range," J. Colloid Interface Sci. **26**, 62–69 (1968).
65. NanoComposix, "NanoComposix: gold metal nanoshells" (2012), retrieved 9 September 2012, http://nanocomposix.com/products/gold/nanoshells.
66. NanoSight, "Nanoparticle size analysis, particle size software, LM10-HS—Products—NanoSight" (2012), retrieved 9 September 2012, http://www.nanosight.com/products/lm10-hs.
67. F. Le, N. Lwin, N. Halas, and P. Nordlander, "Plasmonic interactions between a metallic nanoshell and a thin metallic film," Phys. Rev. B **76**, 165410 (2007).

68. NanoComposix, "NanoComposix products" (2012), retrieved 22 November 2012, http://nanocomposix.com/products.
69. A. Ghadimi, R. Saidur, and H. S. C. Metselaar, "A review of nanofluid stability properties and characterization in stationary conditions," Int. J. Heat Mass Transfer **54**, 4051–4068 (2011).
70. Y. Hwang, J. Lee, C. Lee, Y. Jung, S. Cheong, B. Ku, and S. Jang, "Stability and thermal conductivity characteristics of nanofluids," Thermochim. Acta **455**, 70–74 (2007).
71. J. Tavares and S. Coulombe, "Dual plasma synthesis and characterization of a stable copper-ethylene glycol nanofluid," Powder Technol. **210**, 132–142 (2011).
72. J. U. Kang, "Observation of random lasing in gold-silica nanoshell/water solution," Appl. Phys. Lett. **89**, 221112 (2006).
73. S. Mallidi, T. Larson, J. Tam, P. P. Joshi, A. Karpiouk, K. Sokolov, and S. Emelianov, "Multiwavelength photoacoustic imaging and plasmon resonance coupling of gold nanoparticles for selective detection of cancer," Nano Lett. **9**, 2825–2831 (2009).
74. G. S. Terentyuk, G. N. Maslyakova, L. V. Suleymanova, N. G. Khlebtsov, B. N. Khlebtsov, G. G. Akchurin, I. L. Maksimova, and V. V. Tuchin, "Laser-induced tissue hyperthermia mediated by gold nanoparticles: toward cancer phototherapy," J. Biomed. Opt. **14**, 021016 (2009).